

FE-RICH EJECTA IN THE SUPERNOVA REMNANT G352.7–0.1 WITH *SUZAKU*

A. SEZER*

TÜBİTAK Space Technologies Research Institute, ODTU Campus, Ankara, 06531, Turkey

AND

F. GÖK

Akdeniz University, Faculty of Education, Department of Secondary Science and Mathematics Education, Antalya, 07058, Turkey

The Astrophysical Journal Draft Version June 11, 2014

ABSTRACT

In this work, we present results from a ~ 201.6 ks observation of G352.7–0.1 by using the X-ray Imaging Spectrometer onboard *Suzaku* X-ray Observatory. The X-ray emission from the remnant is well described by two-temperature thermal models of non-equilibrium ionization with variable abundances with a column density of $N_{\text{H}} \sim 3.3 \times 10^{22} \text{ cm}^{-2}$. The soft component is characterized by an electron temperature of $kT_e \sim 0.6$ keV, an ionization time-scale of $\tau \sim 3.4 \times 10^{11} \text{ cm}^{-3} \text{ s}$, and enhanced Si, S, Ar, and Ca abundances. The hard component has $kT_e \sim 4.3$ keV, $\tau \sim 8.8 \times 10^9 \text{ cm}^{-3} \text{ s}$, and enhanced Fe abundance. The elemental abundances of Si, S, Ar, Ca, and Fe are found to be significantly higher than the solar values that confirm the presence of ejecta. We detected strong Fe K-shell emission and determined its origin to be the ejecta for the first time. The detection of Fe ejecta with a lower ionization time-scale favor Type Ia origin for this remnant.

Keywords: X-rays: ISM — ISM: supernova remnants: individual(G352.7–0.1)

1. INTRODUCTION

The Galactic supernova remnant (SNR) G352.7–0.1 was discovered by Clark et al. (1975) in the radio band at 408 and 5000 MHz observations. The remnant has a shell structure with a radio spectral index of $\alpha = -0.6$ (energy flux $S_\nu \sim \nu^\alpha$) and an angular size of 8×6 arcmin² (Green 2009). Dubner et al. (1993) showed the presence of structure of two overlapping rings by using Very Large Array (VLA) image at 1465 MHz.

In the X-ray band, G352.7–0.1 was first detected by Kinugasa et al. (1998) with *ASCA* Galactic Plane Survey Project. The spectra were described by a non-equilibrium ionization (NEI) model with an electron temperature kT_e of ~ 2.0 keV, an ionization parameter τ of $\sim 10^{11} \text{ cm}^{-3} \text{ s}$, an absorption N_{H} of $\sim 2.9 \times 10^{22} \text{ cm}^{-2}$, and overabundances of Si and S. Using the Sedov model and assuming a distance of 8.5 kpc (near to the Galactic center), they estimated an explosion energy of $\sim 2 \times 10^{50}$ erg and an age of ~ 2200 yr.

Giacani et al. (2009) analyzed the *XMM-Newton* observation and reprocessed VLA archival data at 1.4 and 4.8 GHz of G352.7–0.1. They estimated a distance of 7.5 ± 0.5 kpc by studying the interstellar gas surrounding the SNR. Also, using *XMM-Newton* data, they showed the presence of supernova (SN) ejecta in this SNR. The spectra were well fitted with a NEI model with an electron temperature kT_e of ~ 1.9 keV. From spectral fitting they estimated the electron density of the plasma to be $n_e \sim 0.3 \text{ cm}^{-3}$, the age of the remnant to be 4700 yr, the mass of the X-ray emitting gas to be $\sim 10 M_\odot$, and the SN explosion energy to be $\sim 10^{50}$ erg. From the morphology and spectral properties of G352.7–0.1, they concluded that this remnant belonged to the mixed-morphology (MM) class. Toledo-Roy et al. (2014) ex-

plored a blowout scenario to explain the morphological features of G352.7–0.1, presented 3D hydrodynamical simulations of SNR.

Recently, Pannuti et al. (2014) presented X-ray study of the remnant by using data from *XMM-Newton* and *Chandra*. Their *XMM-Newton* spectra gave the best-fit with a single thermal component ($kT_e \sim 1.2$ keV) in NEI condition with enhanced abundances of Si and S. On the other hand, their *Chandra* spectra has been best described with two thermal components (VNEI+VNEI) with temperatures of ~ 2.14 keV for hard and ~ 0.39 keV for soft component for the whole remnant, although the spectra of some regions can be fit with single VNEI model. They obtained overabundant Si and S and confirmed that the X-ray emission comes from ejecta. They also presented the detection of infrared emission from this SNR at $24 \mu\text{m}$ by MIPS aboard *Spitzer*.

G352.7–0.1 is one of Fe-rich SNRs in our Galaxy. Although it has been previously argued to be a core-collapse (CC) SN origin by Giacani et al. (2009) and Pannuti et al. (2014), its progenitor has not been well identified yet. Since *Suzaku* (Mitsuda et al. 2007) has better sensitivity to Fe K-shell lines than other satellites (Yamaguchi et al. 2014), our main aim is to identify the origin of G352.7–0.1 by determining Fe abundance based on a deep observation (~ 201.6 ks) with the X-ray Imaging Spectrometer (XIS; Koyama et al. 2007) onboard *Suzaku*.

The rest of this paper is organized as follows: We present the observation and the data reduction in Section 2. We explain the image and spectral analysis in Section 3. In section 4, we discuss the results and in Section 5, we summarize our conclusions. All through this paper, the errors are given at 90% confidence level.

2. OBSERVATION AND DATA REDUCTION

G352.7–0.1 was observed with the XIS on the focal plane of the X-ray telescope (XRT; Serlemitsos et al.

* aytap.sezer@gmail.com

2007) onboard *Suzaku*, starting on 2012 March 02 at 20:39 (UT) and ending on 2012 March 07 at 13:17 (UT) under the observation ID 506052010. The pointing position was $(l, b)=(352^{\circ}7, -0^{\circ}12)$. The XIS was operated in the normal clocking mode (8 s exposure per frame), with the standard 5×5 or 3×3 editing mode (Koyama et al. 2007). The XIS consists of four sets of X-ray CCD camera systems (XIS0, 1, 2, and 3). XIS1 has a back-illuminated (BI) sensor, while XIS0, 2, and 3 have front-illuminated (FI) sensors. XIS2 has not been functional due to an unexpected anomaly since 2006 November¹. Three out of the four CCD chips were available in this observation: XIS0, XIS1, and XIS3. A fraction of the imaging area of the XIS0 has also been unusable since 2009 June². Each CCD chip contains 1024×1024 pixels (1 pixel= $24\ \mu\text{m}\times 24\ \mu\text{m}$) for a 17.8×17.8 arcmin² field of view (FOV). Two calibration sources of ⁵⁵Fe are installed to illuminate two corners of each CCD for absolute gain tuning.

We used High Energy Astrophysics Software (HEASOFT) package³ version 6.11.1 for the data reduction, XSELECT version 2.4 to extract images and spectra, and the X-ray Spectral fitting package (XSPEC) version 12.7.0 (Arnaud 1996) for the X-ray spectral analysis. The *Suzaku*/XIS calibration database (CALDB: 20130305)⁴ was updated in 2013 March. We downloaded the archival data from the Data Archives and Transmission System (DARTS)⁵. We used the cleaned event file created by the *Suzaku* team. For the spectral analysis, we generated the Redistribution Matrix File (RMF) and Ancillary Response File (ARF) by using the XISRMFGEN and XISSIMARFGEN in the HEASOFT package, respectively (Ishisaki et al. 2007).

3. ANALYSIS

3.1. Imaging analysis

In Figure 1, we show the XIS mosaic image of G352.7–0.1 in the full energy band of 0.3–10.0 keV. To produce the X-ray image, the data of XIS0, XIS1, and XIS3 were added by using XIMAGE package, and the resulting image was smoothed with a Gaussian of $\sigma=3$ arcmin. The solid and dashed circles show the spectral extraction regions (see Section 3.2). We excluded calibration sources at the corners of the CCD chips. X-ray image was overlaid with the VLA radio continuum image (in green contours) of G352.7–0.1 obtained at 4.8 GHz (E. Giacani, private communication).

3.2. Spectral analysis

The XIS spectra of the source were extracted from a circular region with a radius of 3.9 arcmin, centered at $\text{RA}(2000) = 17^{\text{h}}27^{\text{m}}39^{\text{s}}$, $\text{Dec.}(2000) = -35^{\circ}06'49''$ as shown in Figure 1. We extracted background spectrum taken from an annulus region surrounding the remnant (the inner radius 3.9 arcmin and the outer radius is 6.5

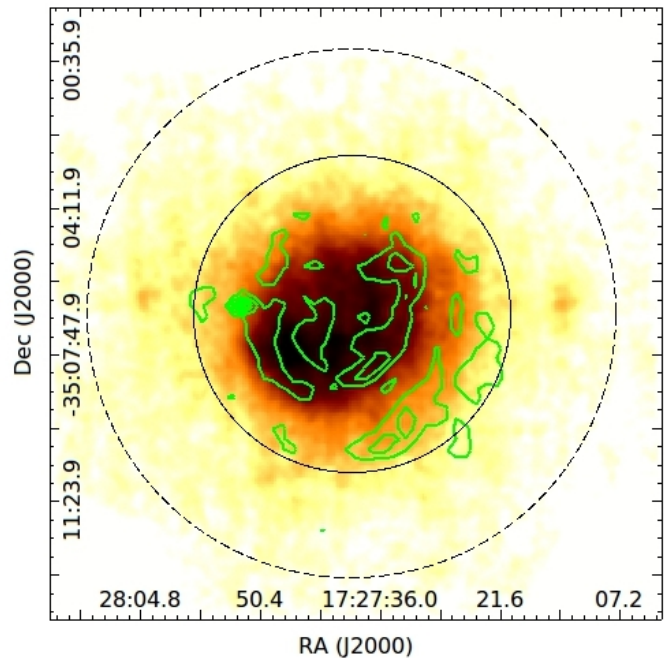


Figure 1. The X-ray image of G352.7–0.1 with the *Suzaku* XIS in the full energy band 0.3–10.0 keV. The image was smoothed with a Gaussian of $\sigma=3$ arcmin. The source and background regions of the X-ray spectra are given by the solid circle with a 3.9 arcmin radius and dashed annulus with a 3.9 and 6.5 arcmin radii, respectively. The radio image at 4.8 GHz band obtained by the VLA observation (Giacani et al. 2009) is overlaid as the contour image in green. The contour levels are 2.54, 5.48, 8.42, and 12.1 mJy beam⁻¹. The corners of the CCD chip illuminated by ⁵⁵Fe calibration sources are excluded from the image.

arcmin) in the same FOV away from the corners containing calibration sources (see Figure 1). We note that the angular size of the remnant is small enough to choose background around it. The spectra were binned to a minimum of 30 counts per bin to allow use of the χ^2 statistic.

We first fitted the spectra with a NEI plasma model (VNEI model with neivers 2.0 in XSPEC; Borkowski et al. 2001) modified by interstellar photo-electric absorption (the wabs component in XSPEC; Morrison & McCammon 1983). The electron temperature (kT_e), the absorbing column density (N_{H}), the ionization time-scale ($\tau=n_e t$), where n_e and t are electron density and the time since the plasma was heated, and the normalization are free parameters, while all elements were fixed at solar abundances (Anders & Grevesse 1989). This model did not give an acceptable fit with a $\chi^2=2509.5$ for 1018 degrees of freedom (d.o.f.). Then, the elemental abundances of Si, S, Ar, Ca, and Fe were also let free while other elemental abundances were fixed to their solar values. In this case, the absorbed VNEI model provided a good fit for the data, with a $\chi^2=1300.9$ for 1013 d.o.f., but failed to reproduce the Fe-K line profile. Residuals of the VNEI spectral fit showed that there was clear residual emission at ~ 6.4 keV. Therefore, we added a Gaussian component (gauss model in XSPEC) to the VNEI model and obtained a statistically acceptable fit with a reduced χ^2 of 1.1 for 1012 d.o.f. We note that the Gaus-

¹ <http://www.astro.isas.jaxa.jp/suzaku/doc/suzakumemo/suzakumemo-2007-08.pdf>

² <http://www.astro.isas.jaxa.jp/suzaku/doc/suzakumemo/suzakumemo-2010-01.pdf>

³ <http://heasarc.nasa.gov/lheasoft/>

⁴ <http://www.astro.isas.ac.jp/suzaku/caldb/>

⁵ <http://www.darts.isas.jaxa.jp/astro/suzaku/>

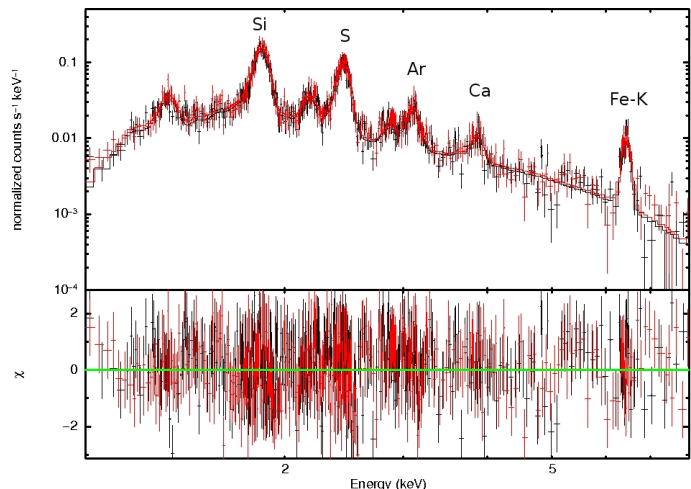


Figure 2. The FI spectra of G352.7–0.1 in the 1.0–8.0 keV energy band was fitted with an absorbed VNEI plus VNEI model. The black and red data points represent XIS0 and XIS3 spectra, respectively. Residuals from the model are plotted in the lower panels.

sian line width parameter was fixed to 0 eV. This fit gave an ionization time-scale of $\sim 2.3 \times 10^{10} \text{ cm}^{-3}\text{s}$, indicating that the plasma is still ionizing. To understand the origin of the Fe line (fluorescence or ejecta), we applied two component NEI model $wabs \times (VNEI + VNEI)$. In this fitting, the electron temperature, ionization time-scale, normalization of both components were let free. The abundances of all elements were fixed at their solar values. This model did not give an acceptable fit with a $\chi^2 = 2509.4$ for 1015 d.o.f. Then, the abundances of Si, S, Ar, and Ca in first component, Fe in second component were free parameters while the others were fixed to their solar values. The fit was significantly improved with a χ^2 of 1.02 for 1010 d.o.f and furthermore yielded the abundance of Fe. Figure 2 shows FI (XIS0 and XIS3) spectra of the G352.7–0.1 fitted simultaneously through an absorbed VNEI+VNEI model in the 1.0–8.0 keV energy band. The best-fit parameters are given in Table 1.

We also calculated the ratios of S, Ar, Ca, and Fe relative to Si and compared them with the Type Ia SN models; carbon deflagration (W7; Nomoto et al. 1997), delayed detonation (WDD2; Nomoto et al. 1997), delayed detonation (DDTe; Badenes et al. 2003), and pulsed delayed-detonation (PDDe; Badenes et al. 2003). We also compared our results with CC SN models (Woosley & Weaver 1995) with different progenitor masses of 11, 12, 15 M_{\odot} and presented them in Table 2.

4. RESULTS AND DISCUSSION

In this paper, we analyzed the X-ray imaging and spectroscopy of a deep *Suzaku* observation of G352.7–0.1. The spectra were well fitted with two-temperature thermal components; the softer component has a plasma temperature of ~ 0.6 keV, while the harder component has plasma temperature of ~ 4.3 keV in NEI. The spectral analysis of this remnant gives us overabundance of Si (4.3 ± 0.4), S (7.0 ± 0.8), Ar (11.1 ± 1.6), Ca (18.8 ± 4.3), and Fe (6.8 ± 0.7) and this state of overabundance confirms that thermal X-ray emission is dominated by ejecta.

The X-ray morphology of G352.7–0.1 was investigated by previous studies with *ASCA*, *XMM-Newton*,

and *Chandra* observation. Using *ASCA* observation Kinugasa et al. (1998) proved that the X-ray emission of the remnant is a shell-type morphology similar to that observed in the radio band. However, *XMM-Newton* image of the SNR showed that the X-ray emission completely fills the interior of the radio remnant; therefore, Giacani et al. (2009) concluded that this remnant belonged to the MM class. Pannuti et al. (2014) confirmed that this SNR is MM by using *XMM-Newton* and *Chandra* data. MM SNRs (Rho & Petre 1998), also known as thermal composites, are identified with shell emission in the radio band and centrally brightened thermal emission in the X-ray band with little or no limb brightening. As seen in Figure 1, XIS image of the G352.7–0.1 in the 0.3–10.0 keV energy band confirms that the SNR has a center-filled X-ray plasma within the radio shell. Although there have been several models to explain MM SNRs (e.g. evaporation model; White & Long 1991 and thermal conduction model; Cox et al. 1999), they are not well understood. Both of the above models suggested that the X-ray emission of MM SNRs is related to the shocked ambient medium, while Slane et al. (2002) were the first to propose that ejecta emission can be non-negligible. The X-ray emission from the ejecta is significant for several MM SNRs (e.g. Lazendic & Slane 2006). Our analysis of *Suzaku* XIS data confirmed that G352.7–0.1 has both MM and ejecta structure. Generally, MM SNRs expand in very dense regions. Most of them interact with molecular clouds and are detected in the γ -ray wavelength. However, neither an OH (1720 MHz) maser nor TeV/GeV γ -ray emission has been detected from this remnant.

MM SNRs are generally in association with molecular clouds, which supports a CC origin for them. However, some MM SNRs have Type Ia origin, such as G272.2–3.2 (Sezer & Gök 2012; Sanchez-Ayaso et al. 2013; McEntaffer et al. 2013) and G344.7–0.1 (Yamaguchi et al. 2012). Moreover, G344.7–0.1 was previously suggested to be a CC SNR; Yamaguchi et al. (2012), however, showed that G344.7–0.1 was originated from a Type Ia explosion by using *Suzaku* data. The progenitor of MM SNR G352.7–0.1 has not been well identified yet. Giacani et al. (2009) favor an origin of a Type II SN, based on the interactions of the SNR with an asymmetric wind. Using *Chandra* observation, Pannuti et al. (2014) argued that it might be a CC, not a Type Ia SN, considering the possibility of a compact central object (CCO) associated with it. In a recent work, Yamaguchi et al. (2014) favored Type Ia origin for this remnant, considering Fe K-shell at ~ 6443 eV line obtained from *Suzaku* data.

From *Suzaku* X-ray spectra of G352.7–0.1, we clearly detected strong Fe K-shell emission which clearly discriminate the progenitor type. One of typical characteristics of Type Ia SNRs is that they contain Fe-rich ejecta in the low ionization state (e.g., RCW 86; Yamaguchi et al. 2011), while the Fe ejecta in CC SNRs is in highly ionized (e.g., Cas A; Maeda et al. 2009) or sometimes in overionized (e.g., W49B; Ozawa et al. 2009) state. The spectra of G352.7–0.1 were modelled by two thermal NEI plasma components (VNEI 1 and VNEI 2) which are super-solar abundant in heavy elements and clearly indicate the ejecta origin of them. The soft component (VNEI 1) consists of Si, S, Ar, and Ca while the

hard component (VNEI 2) consists of only Fe element. The Fe ejecta component is at a temperature ~ 7 times higher and an ionization age ~ 40 times lower than the VNEI 1 component. Considering strong Fe K-shell emission and its being in low ionization state, we conclude that this remnant has been originated from Type Ia explosion. The low ionization age of the hard component indicates that the Fe ejecta was more recently ionized by reverse shock than the Si, S, Ar, and Ca ejecta. In some Type Ia SNRs, low ionization age of Fe ejecta has been detected (e.g., SN 1006: Yamaguchi et al. 2008a; RCW 86: Yamaguchi et al. 2008b; Tycho: Hwang et al. 1998). This fact is explained by the authors as follows: the Fe ejecta has been heated by reverse shock more recently than the other elements, since it concentrates toward the center of the SNR.

We compared the elemental abundance ratio of S/Si ~ 1.6 , Ar/Si ~ 2.6 , Ca/Si ~ 4.4 , and Fe/Si ~ 1.6 with the Type Ia and CC models with different progenitor masses in Subsection 3.2. As seen in Table 2, our abundance ratios are roughly consistent with W7 model in S/Si and Fe/Si, but the abundance ratios of Ca/Si and Ar/Si show a large inconsistency from the model. We obtained a strong Ca abundance from the G352.7–0.1 for the first time, which led to high Ca/Si ratio similar to that found in SNR G337.2–0.7 (Rakowski et al. 2006). Our abundance ratio of Ca/Si is roughly close to PDDe and DDTe models by Badenes et al. (2003), but Ar/Si is about 2-4 times higher than Type Ia models, maybe because of the asymmetric distributions of ejecta. Our abundance pattern seen in the *Suzaku* spectra does not strongly match with Type Ia models.

We estimate some physical parameters of G352.7–0.1 based on the best-fit emission measure, sum of two components $\sim 81.9 \times 10^{56} \text{ cm}^{-3}$. For this purpose, we assume the distance to the SNR to be 7.5 kpc (Giacani et al. 2009) and the plasma is a sphere with radius of $R=3.9$ arcmin. We calculate X-ray emitting volume V to be $\sim 7.6 \times 10^{58} f \text{ cm}^3$ from $V=(4/3)\pi R^3 f$, where f is the filling factor. Then, we estimate the electron density of the plasma n_e to be $\sim 0.36 f^{-1/2} \text{ cm}^{-3}$ (assuming $n_e \sim 1.2 n_H$). From $t=\tau/n_e$ we estimate the age of Fe ejecta plasma, which has a low ionization time-scale of $\tau \sim 8.8 \times 10^9 \text{ cm}^{-3} \text{ s}$, to be $\sim 780 f^{1/2} \text{ yr}$, indicating that Fe ejecta has been heated by reverse shock very recently. Finally, we calculate the mass of the X-ray emitting plasma to be $M_x \sim 23 f^{1/2} M_\odot$ from equation $M_x = n_e m_H V$, where m_H is the mass of a hydrogen atom. The abundances were consistent with super-solar values and derived low X-ray emitting mass ($\sim 23 f^{1/2} M_\odot$) indicate that the plasma is dominated by ejecta material.

5. CONCLUSION

As a result of *Suzaku* XIS analysis, we found that the plasma of G352.7–0.1 is thermal, heavily absorbed with a column density of $\sim 3.3 \times 10^{22} \text{ cm}^{-2}$, consists of a soft component with a plasma temperature of $\sim 0.6 \text{ keV}$ and a hard component with a temperature of $\sim 4.3 \text{ keV}$ in NEI condition. The abundances of Si, S, Ar, Ca, and Fe are found to be enhanced above the solar values confirming the ejecta-dominated nature of G352.7–0.1. We conclude that the origin of the Fe-K emission is Fe-rich

ejecta at high-temperature plasma in a low ionization state and the origin of SN explosion is Type Ia.

We thank Elsa Giacani for providing us with the 4.8 GHz VLA data. AS is supported by TÜBİTAK (The Scientific and Technological Research Council of Turkey) PostDoctoral Fellowship. FG acknowledges support by the Akdeniz University Scientific Research Project Management.

Facilities: Suzaku.

REFERENCES

- Anders, E., & Grevesse, N. 1989, *GeCoA*, 53, 197
 Arnaud, K. A. 1996, in *ASP Conf. Ser.* 101, *Astronomical Data Analysis Software and Systems V*, ed. G. H. Jacoby & J. Barnes (San Francisco, CA: ASP), 17
 Badenes, C., Bravo, E., Borkowski, K.J., & Domnguez, I. 2003, *ApJ*, 593, 358
 Borkowski, K. J., Lyerly, W. J., & Reynolds, S. P. 2001, *ApJ*, 548, 820
 Clark, D. H., Caswell, J. L., & Green, A. J. 1975, *Australian J. Phys. Astrophys. Suppl.*, 37, 1
 Cox, D. P., Shelton, R. L., Maciejewski, W., et al. 1999, *ApJ*, 524, 179
 Dubner, G. M., Moffett, D. A., Goss, W. M., & Winkler, P. F. 1993, *AJ*, 105, 2251
 Giacani, E., Smith, M. J. S., Dubner, G., et al. 2009, *AA*, 507, 841
 Green, D.A. 2009, *Bulletin of the Astronomical Society of India*, 37, 45
 Hwang, U., Hughes, J. P., & Petre, R. 1998, *ApJ*, 497, 833
 Ishisaki, Y., Maeda, Y., Fujimoto, R., et al. 2007, *PASJ*, 59, 113
 Kinugasa, K., Torii, K., Tsunemi, H., et al. 1998, *PASJ*, 50, 249
 Koyama, K., Tsunemi, H., Dotani, T., et al. 2007, *PASJ*, 59, 23
 Lazendic, J. S., & Slane, P. O. 2006, *ApJ*, 647, 350
 Maeda, Y., Uchiyama, Y., Bamba, A., et al. 2009, *PASJ*, 61, 1217
 McEntaffer, R. L., Grieves, N., DeRoo, C., Brantseg, T. 2013, *ApJ*, 774, 120
 Mitsuda, K., Bautz, M., Inoue, H., et al. 2007, *PASJ*, 59, 1
 Morrison, R., & McCammon, D. 1983, *ApJ*, 270, 119
 Nomoto, K., Iwamoto, K., Nakasato, N., et al. 1997, *Nucl. Phys. A*, 621, 467
 Ozawa, M., Koyama, K., Yamaguchi, H., Masai, K., & Tamagawa, T. 2009, *ApJ*, 706, L71
 Pannuti, T. G., Kargaltsev, O., Napier, J. P., & Brehm, D. 2014, *ApJ*, 782, 102
 Rakowski, C. E., Badenes, C., Gaensler, B. M., et al. 2006, *ApJ*, 646, 982
 Rho, J., & Petre, R. 1998, *ApJ*, 503, L167
 Sanchez-Ayaso, E., Combi, J. A., Bocchino, F., et al. 2013, *A&A*, 552, 52
 Serlemitsos, P. J., Soong, Y., Chan, K.-W., et al. 2007, *PASJ*, 59, 9
 Sezer, A., & Gök, F. 2012, *MNRAS*, 421, 3538
 Slane, P., Smith, R. K., Hughes, J. P., & Petre, R. 2002, *ApJ*, 564, 284
 Toledo-Roy, J. C., Velzquez, P. F., Esquivel, A., & Giacani, E. 2014, *MNRAS*, 437, 898
 White, R. L., & Long, K. S. 1991, *ApJ*, 373, 543
 Woosley, S. E., & Weaver, T. A., 1995, *ApJS*, 101, 181
 Yamaguchi, H., Koyama, K., Katsuda, S., et al. 2008a, *PASJ*, 60, 141
 Yamaguchi, H., Koyama, K., Nakajima, H., et al. 2008b, *PASJ*, 60, 123
 Yamaguchi, H., Koyama, K., Uchida, H. 2011, *PASJ*, 63, 837
 Yamaguchi, H., Tanaka, M., Maeda, K., et al. 2012, *ApJ*, 749, 137
 Yamaguchi, H., Badenes, C., Petre, R., et al. 2014, arXiv:1403.5154

Table 1

The Best-fit Spectral Parameters of G352.7–0.1 Through the Use of *Suzaku* Data

Component	Parameters	Values
Absorption	N_{H} (10^{22} cm $^{-2}$)	3.3±0.1
	VNEI 1	
	kT_e (keV)	0.6±0.1
	Si (solar)	4.3±0.4
	S (solar)	7.0±0.8
	Ar (solar)	11.1±1.6
	Ca (solar)	18.8±4.3
	τ (10^{11} cm $^{-3}$ s)	3.4±0.2
	EM^a (10^{57} cm $^{-3}$)	7.4±0.6
VNEI 2	kT_e (keV)	4.3±0.2
	Fe (solar)	6.8±0.7
	τ (10^9 cm $^{-3}$ s)	8.8±0.9
	EM (10^{56} cm $^{-3}$)	7.9±0.4
	χ^2 /d.o.f.	1034/1010
	reduced χ^2	1.02

Notes. The errors are at 90% confidence level.

^aEmission measure $EM = \int n_e n_H dV$, where n_e and n_H are the number densities of electrons and protons, respectively and V is the X-ray-emitting volume.

Table 2

Comparison of the Abundance Ratios with Type Ia Models (W7 and WDD2: Nomoto et al. 1997; PDDe and DDTe: Badenes et al. 2003) and CC Models (Woosley & Weaver 1995)

Element Ratio	Best-fit Abundance Ratio	Type Ia Models				CC Models		
		W7	WDD2	PDDe	DDTe	11 M_{\odot}	12 M_{\odot}	15 M_{\odot}
S/Si	1.63±0.21	1.07	1.17	1.5	1.4	0.87	1.53	0.62
Ar/Si	2.58±0.24	0.89	1.38	0.68	0.60	0.63	1.62	0.50
Ca/Si	4.37±0.32	0.75	0.94	2.9	2.5	0.65	2.04	0.43
Fe/Si	1.58±0.19	1.56	0.85	0.89	0.91	1.37	0.23	0.70